Probing the spin state of spin-crossover complexes on surfaces with vacuum ultraviolet angle-resolved photoemission spectroscopy

Sebastian Rohlf,[†,‡] Jan Grunwald,[¶] Matthias Kalläne,[†,‡] Jana Kähler,[†,‡] Florian Diekmann,[†,‡] Sascha Ossinger,[¶] Benedikt Flöser,[¶] Felix Tuczek,[¶] Kai Rossnagel,[†,‡,§] and Manuel Gruber[*,†,‖]

†*Institut für Experimentelle und Angewandte Physik, Christian-Albrechts-Universität zu Kiel, 24098 Kiel, Germany*

‡*Ruprecht-Haensel-Labor, Christian-Albrechts-Universität zu Kiel, 24098 Kiel, Germany*

¶*Institut für Anorganische Chemie, Christian-Albrechts-Universität zu Kiel, 24098 Kiel, Germany*

§*Ruprecht-Haensel-Labor, Deutsches Elektronen-Synchrotron DESY, 22607 Hamburg, Germany*

‖*Faculty of Physics, University of Duisburg-Essen, 47057 Duisburg, Germany*

E-mail: manuel.gruber@uni-due.de

Abstract

Spin-crossover complexes in direct contact with substrates have sparked considerable interest, in particular in view of their potential applications in molecular electronics. While a huge number of spin-crossover complexes is available, many of them are not robust enough to withstand the sample preparation and/or the interaction with the substrate. The techniques usually employed for these investigations, namely near-edge x-ray absorption fine structure spectroscopy and low-temperature scanning tunneling microscopy, are not adapted for *systematic* studies because of the limited access to synchrotron-radiation facilities and complexity of the (indirect) spin determination, respectively. Here we detail a methodology using a (more) commonly-available technique, namely vacuum ultraviolet (angle-resolved) photoemission spectroscopy, to determine the spin state of layers of three different spin-crossover complexes with thicknesses down to the submonolayer regime. We present an approach to determine the thicknesses of the investigated layers, relying on the inelastic mean free path of electrons determined from combined photoemission and x-ray absorption measurements. We report on the high-spin to low-spin relaxation dynamics of SCO layers and the influence of the ultraviolet light on these dynamics. While the observed relaxation processes occur on a timescale on the order of minutes, probing spin-state dynamics on the picosecond timescale is foreseeable with pump-probe photoemission spectroscopy.

Keywords

Spin crossover, photoemission spectroscopy, spin state, TMDC, submonolayer

Introduction

Spin-crossover (SCO) complexes have attracted considerable attention over the last decades, with numerous potential applications exploiting their intrinsic spin-state bistability.[1–6] The deposition of such compounds on substrates[7–26] promises functional surfaces, where, for instance, various optical, electric, and magnetic properties of the surface may be achieved by switching the complexes. Electrical control and readout of SCO in nanodevices, in which a SCO layer is in contact with electrodes, is of particular interest.[27–30] However, obtaining functional SCO molecules in direct contact with surfaces is associated with difficulties[31–37] such that only few successful cases have been reported so far.[38–49] SCO complexes may fragment upon sublimation, which is the deposition method of choice for the preparation of clean molecular layers. In addition, the interaction between the complexes and the substrate

may lead to fragmentation or loss of functionality of the complexes.[31–37] The conservation of the molecular integrity and functionality upon sublimation and interaction with a given substrate is currently challenging to predict, such that systematic experimental studies are required. We note that the deposition of SCO nanoparticles, *e. g.* using matrix-assisted laser evaporation, is also associated with similar difficulties.[50,51]

Besides the problems inherent to the materials, investigating SCO layers down to the submonolayer regime on surfaces demands adapted instrumentation. So far, near-edge x-ray absorption fine structure (NEXAFS) spectroscopy[16,36,37,39–41,45,49,52,53] and low-temperature scanning tunneling microscopy (STM)[16,32,34,35,39,42,44,54,55] are methods of choice for studying submonolayer coverages of SCO complexes on surfaces. While providing the necessary selectivity and sensitivity, application of these methods is not trivial, as recently reviewed,[37] which can complicate the interpretation of the data. In addition, NEXAFS measurements of SCO systems can so far only be performed in large-scale facilities with limited access. On the other hand, STM measurements do not always provide clear evidence for spin switching (indirect determination) and are relatively slow in comparison to those performed with NEXAFS. For these reasons, along with technical issues, STM does not appear to be a method of choice for *systematic* investigations of a large variety of SCO complexes. In particular, STM may not be adapted for systematic determination of the spin state as a function of the sample temperature and illumination intensity.

Here, we show that vacuum ultraviolet angle-resolved photoemission spectroscopy (VUV-ARPES) can be employed for a *quantitative* spin-state determination of SCO complexes in layers on surfaces. Using laboratory-based instrumentation, we characterized layers of various thicknesses composed of three different SCO compounds. In particular, reliable spin-state determination of submonolayer samples is evidenced. Besides temperature- and light-induced transitions, spin switching can be effectively triggered by the ultraviolet illumination at low temperatures, in analogy to the soft x-ray-induced excited spin state trapping (SOXIESST) observed with x-rays.[52,56]

Methods

SCO compounds Three compounds were investigated, namely $[Fe(H_2B(pz)_2)_2(phen)]$ ($H_2B(pz)_2$ = dihydrobis(pyrazolyl)borate, phen = 1,10−phenanthroline), $[Fe(pypyr(CF_3)_2)_2(phen)]$ (pypyr =2−(2′−pyridyl)pyrrolide), and $[Fe\{H_2B(pz)(pypz)\}_2]$ (pz = pyrazole, pypz = pyridylpyrazole), hereafter respectively referred to as Fe-Bpz (Fig. 1b), Fe-pypyr (Fig. 1c) and Fe-Bpzpypz (Fig. 1d). These complexes were synthesized as described in Refs. 17,25,57.

Preparation of the samples 1T-$TiTe_2$ and 1T-HfS_2 are composed of covalently bonded chalcogen-metal-chalcogen sandwich layers with weak van der Waals-like forces between these layers. Atomically flat and chemically saturated surfaces were obtained by Scotch-tape cleaving the crystals along the basal plane at a pressure below 10^{-7} mbar. The complexes were deposited onto the clean substrates by sublimation in ultrahigh vacuum (UHV) from a Knudsen cell heated to 160 °C, 165 °C and 145 °C for Fe-Bpz, Fe-pypyr and Fe-Bpzpypz, respectively.

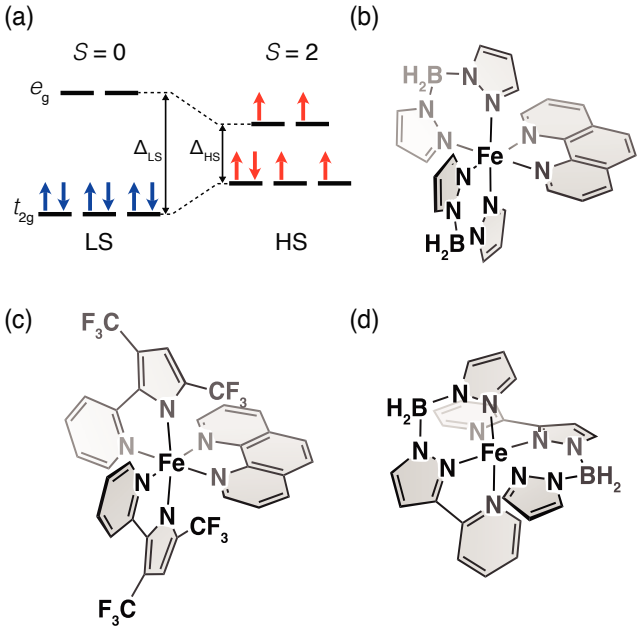

Figure 1: (a) Schematic of the occupation of the d orbitals of Fe^{2+} SCO compounds in the LS and HS states. Molecular structures of (b) Fe-Bpz, (c) Fe-pypyr and (d) Fe-Bpzpypz.

VUV-ARPES and UP measurements The measurements were partly carried out at the ASPHERE III experimental station (DESY, Hamburg) equipped with a VG Scienta DA30 hemispherical analyzer. A BALZERS He discharge lamp was used as photon source. Complementary measurements were performed at a photoemission experiment (IEAP, Kiel University) with a VG Scienta R4000 hemispherical analyzer and a Specs UVS 300 VUV light source. Energy and angular resolution of the analyzers at both experiments were set to 40 meV (pass energy E_P = 20 eV, entrance slit width 0.8 mm) and 0.1 °, respectively. For the variable VUV photon flux measurements, the toroidal mirror monochromator in front of the Specs light source was detuned. Note that the monochromator only selects the He-Iα spectral line, a detuning does not affect the photon energy ($h\nu$ = 21.22 eV). Most of the acquired VUV-ARPES data were integrated over the emission angle (surface-parallel momentum component $k_\parallel$), such that they effectively are equivalent to ultraviolet photoemission (UP) spectroscopy data. We may therefore equivalently refer to UP or VUV-ARPES spectra.

Illumination with a laser For the LIESST

experiments, a 532 nm laser with an intensity of 1.35 mW mm^{-2} on the sample surface was used. A large laser beam diameter of 5 mm ensures spatial overlap with the VUV light spot (1 mm).

DFT calculations Calculations of the single molecules in the gas phase were carried out with the ORCA software package.[58,59] The crystallographic structures of Fe-Bpzpypz[24] and Fe-Bpz[57] were used as a starting point. The structure of Fe-pypyr was pre-optimized using molecular mechanics with the UFF[60] force field as implemented in Avogadro,[61] followed by geometry optimization with semiempirical methods (PM7[62]) implemented in MOPAC2016.[63]

Geometry optimizations were performed with ORCA at the B3LYP[64–66]/def2-SVP[67,68] level with the D3BJ dispersion correction,[69,70] the RIJCOSX approximation, fine numerical integration grids (grid4 and gridX4 in ORCA nomenclature), and the CG solver. The orbitals and their energy were calculated with ORCA at the B3LYP*[71]/def2-QZVP[67,68] (* ScalHFX = 0.092024) level with the RIJCOSX approximation, and fine numerical integration grids.

Results and discussion

The switching between the low-spin (LS) and high-spin (HS) states of SCO compounds is associated with a rearrangement of the electrons in the d orbitals (Fig. 1a), which leads to a spin-state dependent electronic structure. This is, in particular, exploited by NEXAFS spectroscopy, essentially sensitive to unoccupied states, to infer the spin state of the investigated complexes.[16,36,37,39–41,45,49,52,53,72] Alternatively, spin-state determination may be realized using VUV-ARPES and more generally UP spectroscopy, which are sensitive to the occupied states of the molecules.[10,21] A drastic difference between the two methods is that NEXAFS probes orbitals related to a given element, *e. g.* Fe where the expected change is the largest, while VUV-ARPES/UP spectroscopy is sensitive to all elements, diluting to some extent the signal useful to monitor the molecular spin state. Nonetheless, Ludwig *et al.*[10] have shown that the spin state of a 7 nm thick film of Fe-Bpz (Fig. 1b) on Au(111) can be determined in a semi-quantitative manner using UP spectroscopy. Poggini *et al.*[21] have reported (small) changes of the UP spectra associated with spin switching.

In the following we show that the spin-state sensitivity of UP spectroscopy is not limited to these two examples but appears to be generally applicable for Fe^{2+} SCO compounds. We introduce a method to quantitatively determine the fraction of HS molecules and demonstrate that VUV-ARPES can be employed to probe SCO complexes down to sub-monolayer coverages.

The apparent generality of the LS feature

Fig. 2a shows angle $k_{\parallel}$-integrated VUV-ARPES spectra of a 30 ML thick film of Fe-Bpz on 1 T-$TiTe_2$ acquired under experimental conditions for which the complexes are known to be in the LS state (upper blue curve; 120 K) and in the HS state (upper red curve; 28 K under illumination with a 532 nm laser), respectively. The spectra are very similar to those obtained for the same compound on Au(111) (Ref. 10) except for an energy offset attributed to thickness-dependent charging of the layer. This similarity is expected as the probing depth of VUV-ARPES, on the order of 1–3 ML, is smaller than the molecular film thickness, leaving the spectra void of substrate features.

While the LS and HS spectra for each compound in Fig. 2a appear to be relatively similar over the entire energy range $[-8, 0]$ eV, the first feature below the Fermi level is drastically different in the LS and HS state (see inset to Fig. 2a). The intensity of the peak in the LS state is almost twice as high as the one in the HS state, which makes it a clear fingerprint of the spin state. Owing to its spin-state dependence and its dominant intensity in the LS state, the first feature below the Fermi level is hereafter referred to as the *LS feature*. The LS feature is not limited to Fe-Bpz, but also present for Fe-pypyr and Fe-Bpzpypz (Figs. 2b–c), which suggests that this feature is a general property of Fe^{2+} SCO compounds.

Gas-phase DFT calculations have been performed for the three compounds in the LS and in the HS states. The energies of the occupied molecular orbitals (MOs) are shown in the bottom of Figs. 2a–c. For a better comparison with the experimental results, each transition from a MO is described by a normalized Gaussian function with a standard deviation of 0.35 eV, and the sums of the Gaussian functions represent simulated spectra (bottom red and blue curves in Figs. 2a–c). The different peaks in the simulated spectra are tentatively associated to the peaks of the experimental spectra (see dashed lines in Figs. 2a–c). Interestingly, the calculations reproduce the LS feature, *i. e.* the first feature below the Fermi level is significantly more intense in the LS state than in the HS state. This may be understood by considering the density of MOs. While the highest occupied MO of the HS state is the closest to the Fermi level, it is distant from the other MOs. In contrast, the three highest occupied MOs of the LS state are close in energy, doubly occupied and thus lead to a higher *density* of states.

From these measurements on three compounds, we extrapolate that the LS feature is a generic property of Fe^{2+} SCO complexes, which may in principle be used to monitor the fraction of HS molecules in a sample. We, however, note that the LS features exhibit small differences from compound to compound (slightly different energies and widths).

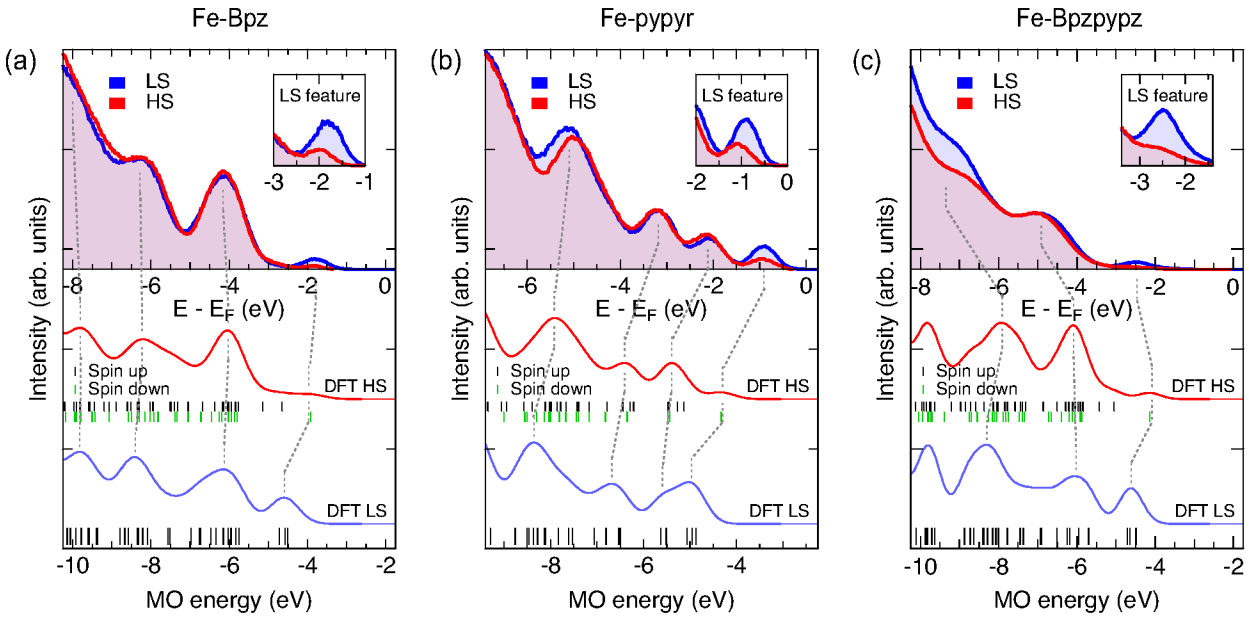

Figure 2: Photoemission spectra of (a) $\sim$ 30 ML Fe-Bpz on 1 T-$TiTe_2$, (b) $\sim$ 40 ML Fe-pypyr on 1 T-$TiTe_2$ and (c) $\sim$ 17 ML Fe-Bpzpypz on 1 T-HfS_2 acquired at 21 - 28 K under illumination with a 532 nm laser (upper red curves) and at 120 K (upper blue curves). Under these experimental conditions, the complexes are respectively in the HS (red) and in the LS (blue) state. The first spectral signature below the Fermi level, empirically referred to as the LS feature, is emphasized in insets. The vertical bars in the lower part of the panels represent MOs, inferred from gas-phase DFT calculations, whose energies depend on the spin state. In the LS state (bottom) the orbitals are doubly occupied while the orbitals are spin split in the HS state (black and green bars for spin up and down, respectively). For better comparison with the experiments, each transition from a MO is described by a normalized Gaussian function with a standard deviation of 0.35 eV. The sums of these Gaussian functions lead to the spectra denoted DFT HS (red) and DFT LS (blue) in the lower part of the panels. Broken dashed lines tentatively associate the features in the experimental and calculated spectra.

Spin-state determination of multilayer samples

A determination of the spin state based on a linear combination of HS and LS reference spectra, in analogy to what has been done using NEXAFS,[37,39–41,45,49,52,53] is in principle also possible for UP spectra. HS and LS reference spectra for each compound are acquired at $\approx$25 K with laser illumination and at 120 K, respectively (Fig. 2). Denoting $I_{LS}(E)$ and $I_{HS}(E)$ the intensities of the LS and HS reference spectra at binding energy E, the spectral intensity $I(E)$ is approximated using

$$I(E) = A \cdot [\gamma_{HS} \cdot I_{HS}(E - E_{\text{off}}) + (1 - \gamma_{HS}) \cdot I_{LS}(E - E_{\text{off}})], \quad (1)$$

where γ_{HS}, E_{off} and A are respectively the fraction of HS molecules, an energy offset, *e. g.* taking into account a potential charging of the layer, and a factor accounting for variation of the VUV intensity. It should be emphasized that, owing to the small inelastic mean free path of the photo-excited electrons ($\approx$ 0.4–3 nm at a kinetic energy of 10–20 eV[73]), most of the signal in the UP spectra originates from the topmost molecular layers. Therefore, HS fractions inferred from Eq. 1 may not be representative of the entire film in the case of an inhomogeneous spin transition.

An example of a fit with Eq. 1 (black curve) is shown in Fig. 3a for an UP spectrum acquired at 28 K on 40 ML Fe-pypyr on 1 T-$TiTe_2$ (green curve) yielding a HS fraction of 34 ± 3 %. The agreement is relatively good. Importantly, the energy range over which the fitting is done is not limited to the LS feature as the outcome would be sensitive to (small) variation in the VUV-light intensity. Too large energy intervals, such as shown in Figs. 2a–c, are not adapted either. Variations of the photoemission intensity for binding energies $|E_B| > 5$ eV were monitored as a function of time (several hours) presumably due to the adsorption of gaseous molecules of the UHV environment. We empirically found that fits over the first two photoemission features (−3 to 0 eV for Fe-pypyr) provide reliable estimates of the fraction of HS molecules. The signal of both features allows to account for variations in the VUV-light intensity, while the spin-state readout is mostly inferred from the LS feature.

To show the sensitivity of the method, we induced spin transitions in the molecular layer by changing the temperature and illuminating the sample with a 532 nm laser (Fig. 3c). The Fe-pypyr sample exhibits a HS fraction of $\approx$ 30 % at room temperature that evolves

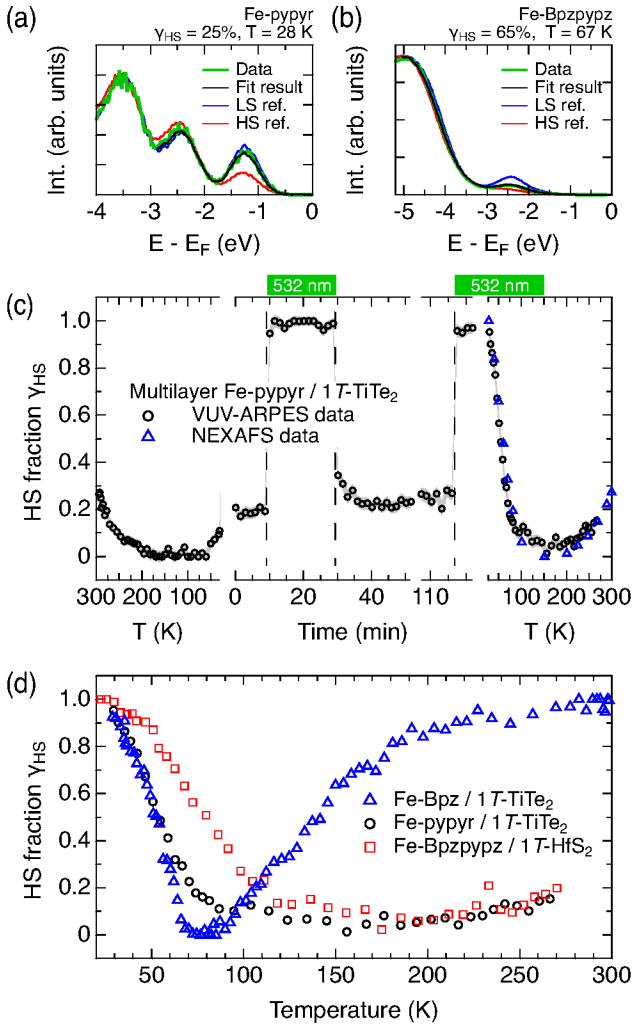

Figure 3: UP spectra measured at (a) 28 K on 40 ML Fe-pypyr on 1 T-$TiTe_2$ (no light irradiation) and (b) at 67 K on 17 ML Fe-Bpzpypz on 1 T-HfS_2 (532 nm laser light irradiation) along with fits to Eq. 1 (black) using the HS (red) and LS (blue) reference spectra obtained from Figs. 2b–c. The fits yield fractions of HS molecules of (a) 25 and (b) 65 %. (c) Evolution of the HS fraction as a function of temperature and time (at 21 K) of 40 ML Fe-pypyr on 1 T-$TiTe_2$ (black circles). Green rectangles indicate the time during which a 532 nm laser illuminated the sample. HS fractions inferred from NEXAFS measurements on a similar sample are overlaid (blue triangles, see Ref. 36 for experimental details). (d) HS fraction *versus* temperature of Fe-Bpz, Fe-pypyr and Fe-Bpzpypz during 532 nm laser light irradiation.

toward zero as the temperature is lowered. For temperatures below 60 K, the HS fraction increases again, up to ≈ 20 %. In analogy to the light-induced excited spin state trapping[74] (LIESST) and the soft-x-ray induced spin state trapping[14,19,52,53,56] (SOXIESST), the VUV light induces transitions from the LS to the HS state[10] (VUVIESST). Illumination of the sample at 28 K with green light leads to a drastic change of the HS fraction to values close to 100 % (see γ_{HS} at ≈ 10 min). The HS fraction takes back its previous values of 20–30 % upon switching the illumination off (see γ_{HS} at ≈ 30 min). This series of measurements evidences that spin-state determination as proposed in this section is indeed sensitive to the spin state of the molecular layer. Moreover, the method is quantitative and provides estimates of γ_{HS} comparable to those inferred from NEXAFS measurements. This is illustrated on the right-hand side of Fig. 3c. The HS fraction evolves from ≈ 100 % toward zero as the sample is warmed up under illumination (black circles) because the LIESST effect becomes less and less effective. Then, between 100 K and 300 K, thermally induced LS-to-HS transitions lead to a slow increase of γ_{HS}. Data inferred from NEXAFS measurements[36] are overlaid (blue triangles). The evolutions of γ_{HS} obtained with the two techniques are identical within the precision of the data, which *a posteriori* validates the method presented here.

The determination of the HS fraction is not limited to Fe-pypyr but can be extended to other complexes. Fig. 3b shows UP spectra of 17 ML Fe-Bpzpypz on 1 T-$TiTe_2$ at 44 K (green), 150 K (blue, labeled LS) and 21 K plus green illumination (red, labeled HS). A fit of the data using Eq. 1 (black) reproduces the data relatively well (green). It may be noted that the signal-to-noise ratio of the data in Fig. 3b is significantly better than that in Fig. 3a owing to approximately four times better photoelectron-counting statistics.

Fig. 3d summarizes the evolution of γ_{HS} with temperature of multilayers of the three investigated SCO compounds, namely Fe-Bpz (triangles), Fe-pypyr (circles) and Fe-Bpzpypz (squares) during 532 nm laser light illumination. Determination of HS fractions from UP spectra appears to be reliable and generally applicable to Fe^{2+} SCO compounds. In particular, the accuracy of the inferred HS fractions is comparable to that obtained in NEXAFS measurements as evidenced in Fig. 3c.

Spin-state determination of sub-ML samples

Visibility of the LS feature

The contribution of the substrate to the signal increases more and more as the thickness of the molecular layer decreases. For sub-ML coverages, the photoemission signal originating from the molecular layer is generally orders of magnitude lower than that of the substrate, and effectively contained in the noise of the data. In NEXAFS experiments, this issue is significantly less pronounced owing to the element selectivity of the method.

This problem is illustrated in Figs. 4a–c. The photoemission map of a Au(111) sample, often used as a substrate for the investigation of SCO systems, exhibits a significant intensity below the Fermi level over several eV (Fig. 4a). The photoemission intensity distribution is only marginally affected by the deposition of 0.5 ML Fe-pypyr (Fig. 4b). In particular, no LS feature is dis-

cernible (expected at $E - E_F \approx -1\,\mathrm{eV}$). To better compare the data before and after deposition of Fe-pypyr, the intensity is integrated over $k_\parallel$ leading to the spectra shown in Fig. 4c. The $I(E - E_F)$ spectrum acquired on the sub-ML sample (black curve) is very similar to that of the substrate (gray area), at least for binding energies of less than 2 eV. In contrast, for larger binding energies, the molecular sub-monolayer decreases the signal originating from the substrate. As will be shown below, the molecule-induced attenuation of the substrate signal can be used to calibrate the thickness of the molecular layer.

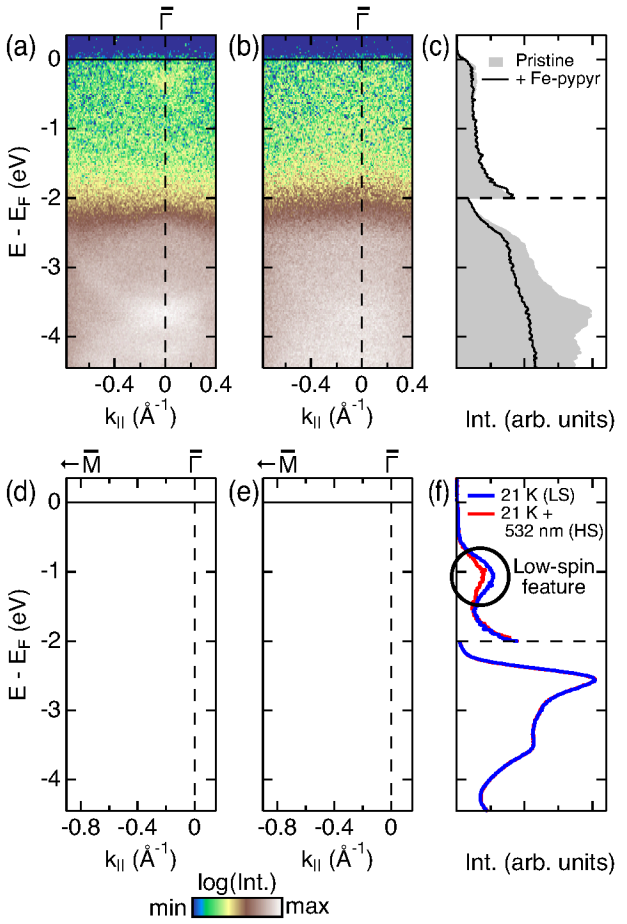

Figure 4: VUV-ARPES data of (a) a pristine Au(111) and (d) 1T-HfS_2 substrate. The photoemission intensity is encoded in the color (see color scale at the bottom). (b) and (e) ARPES images upon deposition of 0.5 ML of Fe-pypyr on the Au(111) and 1T-HfS_2 substrates, respectively. (c) Spectra obtained by integrating over $k_\parallel$ the intensities shown in (a) (light gray area) and in (b) (dark curve). (f) $k_\parallel$-integrated VUV-ARPES spectra of 0.5 ML Fe-pypyr on 1T-HfS_2 at 21 K with (red) and without (blue) green illumination. The intensities are respectively multiplied by a factor of 5 and 20 in (c) and (f) for energies $|E - E_F| < 2\,\mathrm{eV}$ (above the horizontal dashed line). The data shown in (a–e) were acquired at room temperature.

Yet, the non-visibility of the LS feature may be circumvented by an adequate choice of the substrate. In essence, the substrate density of states should be relatively low at the energy of the LS feature. For instance, the semi-conducting substrate 1T-HfS_2 has a large band gap of 2.85 eV.[75] Corresponding photoemission maps show a negligible intensity from −2 eV to 0 eV (blue area in Fig. 4d). In this case, deposition of 0.5 ML of Fe-pypyr significantly changes the photoemission map, at least at energies close to the LS feature (see green area at $E - E_F \approx -1\,\mathrm{eV}$). The LS feature is also evident in UP spectra obtained by integrating over the $k_\parallel$ component in the photoemission maps. Fig. 4f shows two such spectra acquired at 21 K with (red) and without (blue) illumination with a 532 nm laser. As expected, the intensity of the LS feature decreases as complexes are converted from the LS to the HS state.

We emphasize that such measurements on sub-ML coverages of SCO complexes are not limited to the 1T-HfS_2 substrate, but can be extended to other materials exhibiting a band gap in the region of interest. In particular, the band gap may be a projected band gap, only covering a (small) range of $k_\parallel$. The conversion from map to spectra such as in Figs. 4b,c,e,f would then be performed by integrating $k_\parallel$ over an adequate range. This would, for instance, make highly oriented pyrolytic graphite (HOPG) an adequate substrate for the investigation of sub-ML coverages of SCO complexes using VUV-ARPES.

Determination of the HS fraction

As described above, the determination of the HS fraction in multilayer samples (Eq. 1) involves not only the LS feature but also a second molecular feature. The combination of both molecular features effectively scales the spectra to be insensitive to VUV-light intensity variations. For sub-ML coverages, the LS feature is, however, the only molecular feature distinctly visible in the UP spectra because of the limited band gap of the substrate. The intensity of this feature I_{mol} is measured by integrating the photoemission signal in a 0.6 eV energy range around the maximum of the feature (at 1.1 eV for Fe-pypyr on 1T-HfS_2) to be less sensitive to noise. To scale the LS feature, we use I_{sub} the intensity of the substrate integrated from −4.5 to −2 eV. The normalized LS-feature intensity $I' = I_{\mathrm{mol}}/I_{\mathrm{sub}}$ is a readout of the spin state of the molecular layer. Denoting I'_{LS} and I'_{HS} the normalized intensities of respectively LS and HS reference spectra, the HS fraction is given by:

$$\gamma_{\mathrm{HS}} = \frac{I'_{\mathrm{LS}} - I'}{I'_{\mathrm{LS}} - I'_{\mathrm{HS}}}. \qquad (2)$$

For HS and LS references, we use spectra acquired on the same sample exhibiting the smallest and largest LS feature, respectively. This method therefore gives the *relative* change of the HS fraction for samples experiencing a partial spin transition. It may be worth mentioning that the determination of the HS fraction from linear combinations of HS and LS reference spectra (Eq. 1), including both molecule and substrate features, turned out unsuccessful. Besides the expected temperature-

dependence of the LS feature, the spectrum of the substrate exhibits (small) variations upon changes of temperature, and may therefore not be employed as a reference for photon intensity. The integrated intensity I_{sub} is, however, effectively independent of temperature. This is why we rely on Eq. 2 rather than on Eq. 1 to determine the fraction of HS molecules of ultrathin molecular layers.

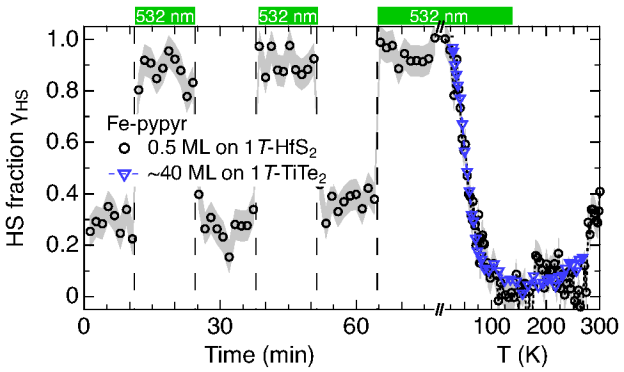

Figure 5: Evolution of the HS fraction as a function of time (at 21 K) and temperature of 0.5 ML Fe-pypyr on 1 T-HfS_2 (black circles) and of 40 ML Fe-pypyr on 1 T-$TiTe_2$ (blue triangles). The green rectangles on top indicate the measurements performed under illumination with a 532 nm laser. The gray area indicates a 7 % uncertainty inferred from the variations in the expected steady-state γ_{HS}.

Fig. 5 shows the HS fraction of 0.5 ML Fe-pypyr on 1 T-HfS_2, derived from Eq. 2, as a function of time and temperature. At the start of the time series at 21 K, the HS fraction is $\approx 25\,\%$ owing to VUVIESST. To demonstrate the sensitivity of the HS-fraction determination method presented here, light-induced LS-to-HS transition and subsequent (partial) relaxation to the LS state are triggered by turning on and off 532 nm laser illumination. γ_{HS} follows the expectations, evolving between $\approx 30\,\%$ and $\approx 90\,\%$ as the illumination is switched on and off, respectively (see green rectangles at the top of Fig. 5). The estimates of the HS fraction with ($\approx 90\,\%$) and without green illumination ($\approx 30\,\%$) of 0.5 ML Fe-pypyr on 1 T-HfS_2 are very similar to those found in the multilayer samples ($\approx 100\,\%$ and $\approx 25\,\%$, see Fig. 3c), highlighting the negligible impact of the 1 T-HfS_2 substrate on the SCO properties, as previously reported.[36]

The right part of Fig. 5 displays γ_{HS} as a function of temperature. From 21 K to approximately 150 K, the HS fraction decreases as the LIESST effect becomes less and less efficient. Upon further increasing the temperature (150 K to 300 K), an increasing fraction of the complexes exhibits a LS-to-HS thermal transition.

The dependence of γ_{HS} on temperature for 40 ML Fe-pypyr on 1 T-$TiTe_2$ is included in the figure (see blue triangles in Fig. 5). The evolutions of the sub-ML and multilayer are identical within the uncertainty of the measurements. The comparison of the two data sets in Fig. 5 validates *a posteriori* that Eq. 2 provides reliable and quantitative estimates of the HS fraction.

The data shown in Fig. 5 illustrate that VUV-ARPES is a viable tool to investigate the SCO properties of sub-ML molecular coverages on surfaces. VUV-ARPES may be seen as a laboratory-based alternative to NEXAFS, giving similarly reliable estimates of γ_{HS}.

Investigation of 0.7 ML Fe-Bpzpypz

Having validated the method, we now employ it to investigate a new system, namely 0.7 ML Fe-Bpzpypz on 1 T-HfS_2. As for Fe-pypyr on 1 T-HfS_2, the photoemission intensity for $-2 \leq E - E_F \leq 0$ eV, initially negligible for the bare 1 T-HfS_2 substrate (bluish area in Fig. 6a), increases as Fe-Bpzpypz molecules are deposited giving rise to the LS feature (see horizontal greenish area in Fig. 6b). The fraction of HS molecules was deduced from photoemission maps, such as the one shown in Fig. 6b, using the method described above. We observe a HS fraction of 35 % at 300 K (not shown), decreasing toward zero as the temperature is reduced. Fig. 6c shows the evolution of the HS fraction as a function of increasing temperature during illumination with green laser light. At the lowest temperature, the molecules are excited toward the HS state because of the LIESST effect. With increasing temperature the HS fraction is decreasing toward almost zero at 150 K. The evolution of γ_{HS} with temperature and illumination evidences that the Fe-Bpzpypz complexes are intact and functional in direct contact with the 1 T-HfS_2 substrate.

Data acquired on a thicker Fe-Bpzpypz film (17 ML) are overlaid in Fig. 6c (squares). The HS-fraction evolution of the sub-ML and multilayer samples are essentially the same, pointing out the negligible impact of the 1 T-HfS_2 substrate. It is worth mentioning that, in the absence of green illumination, a HS fraction of $\approx 75\,\%$ is obtained at 21 K (not shown) because of the VUVIESST effect. In comparison, under similar experimental conditions, Fe-Bpz and Fe-pypyr exhibit HS fractions of 65 (Ref. 10) and 30 %, respectively. Out of the three compounds investigated in this study, Fe-Bpzpypz is therefore the one which is the most sensitive to VUVIESST.

Determination of the film thickness

An accurate determination of the film thickness in the sub-ML range using ARPES is difficult. Nonetheless, this is not very much different from other spectroscopic techniques, such as NEXAFS as recently reviewed.[37] In the following, we discuss in detail how the thickness is determined along with the underlying assumptions.

Above, we already mentioned that the deposition of 0.5 ML Fe-pypyr on Au(111) leads to an attenuation of the Au(111) signal. This is because photoelectrons originating from the substrate interact with the molecular layer, and are reflected back to the sample and/or lose energy so that they contribute to the background or cannot escape the sample anymore. In the limit of low molecular thicknesses and under the assumption of a layer-by-layer growth, the photoelectron intensity orig-

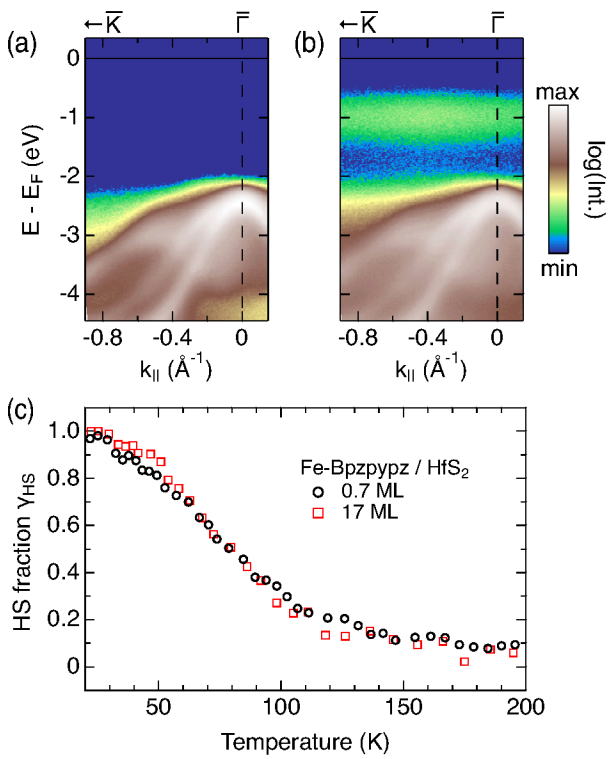

Figure 6: Photoemission intensity maps of $1T$-HfS_2 (a) without and (b) with an overlayer of 0.7 ML Fe-Bpzpypz. (c) Evolution of the HS fraction as a function of temperature of 0.7 ML (circles) and 17 ML (squares) Fe-Bpzpypz on $1T$-HfS_2 during illumination with a 532 nm laser. Temperatures are accurate to within ±8 K.

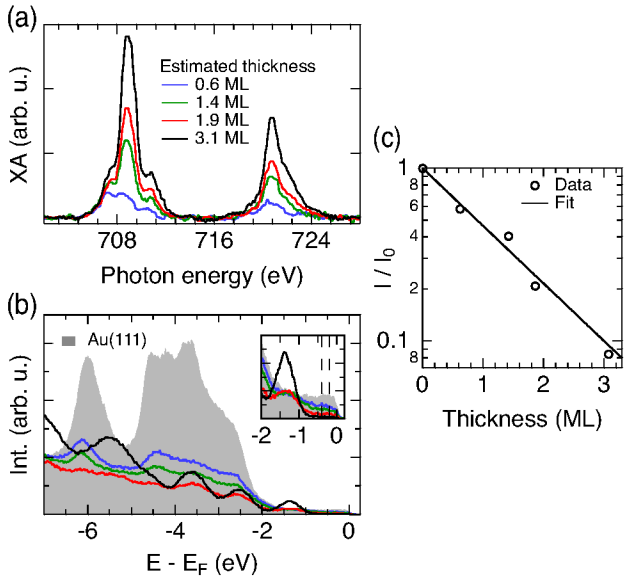

Figure 7: (a) Background-subtracted x-ray absorption (XA) spectra of four Fe-pypyr layers of varying thicknesses on Au(111). (b) VUV-ARPES spectra acquired on the very same samples as in (a) with the same color coded thicknesses along with a spectrum acquired on a clean Au(111) surface (gray area). The inset is a zoom of the spectra for $-2\,\mathrm{eV} \leq E - E_F \leq 0\,\mathrm{eV}$. Dashed vertical lines show the lower and upper bounds of the interval over which the intensity is integrated, leading to I. (c) I/I_0 *versus* the thickness of the molecular layer, where I_0 corresponds to the integrated intensity of the clean substrate. The experimental data (circles) of the three smallest thicknesses are fitted using Eq. 3 (black curve) leading to $\lambda = 1.3 \pm 0.1$ ML. All spectra were acquired at room temperature.

inating from the substrate is given by:

$$I(d) = I_0 \cdot \exp\left(-d/\lambda\right), \qquad (3)$$

where I_0 is the photoelectron intensity from the substrate (without molecules) and d the thickness of the molecular layer. $\lambda(E_{\mathrm{kin}})$ describes the energy dependent inelastic mean free path of the photoelectrons in the molecular layer. Note that λ is the analogue of the electron mean escape depth of NEXAFS experiments, with the key difference that they are related to electrons of different energy ranges (∼ 10–30 eV *versus* ∼ 100–1000 eV). The thickness d may be retrieved using Eq. 3 provided that λ is known.

To the best of our knowledge, no experimental estimates of $\lambda(E_{\mathrm{kin}} \approx 10\text{–}20\,\mathrm{eV})$ for layers of SCO complexes have been reported so far. In the following, we provide such an estimate by measuring the ratio I/I_0 for different thicknesses d of Fe-pypyr on Au(111). The main difficulty resides in knowing the thickness d of the investigated molecular films. We combined VUV-ARPES and NEXAFS measurements on the very same samples and in the same experimental station allowing us, on one hand, to measure the ratio I/I_0, and, on the other hand, determine the thickness d of the layer. Relative thicknesses are inferred from the NEXAFS spectra (Fig. 7a) using Eq. 12 of Ref. 37. An absolute thickness determination of the lowest thickness is obtained by comparing the integrated edge-jump (Eq. 9 of Ref. 37) of the corresponding NEXAFS spectrum (blue curve in Fig. 7a) to the one of the same system measured at another beamline and calibrated using scanning tunneling microscopy.[36] In other words, we use the formalism developed for NEXAFS spectroscopy[37] to determine the thicknesses of the four molecular films (0.6, 1.4, 1.9 and 3.1 ML).

Fig. 7b shows VUV-ARPES spectra acquired on the very same samples measured in Fig. 7a. In the energy range from −0.4 to −0.2 eV (see dashed lines in Fig. 7b), the intensity decrease toward zero with increasing thicknesses indicates that most of the signal originates from the substrate. The intensity integrated over this energy range I normalized over the integrated intensity of the substrate I_0 is plotted in Fig. 7c as a function of the molecular layer thickness. A fit of the data points to Eq. 3 (black curve) leads to $\lambda = 1.3 \pm 0.1$ ML.

With the knowledge of λ, the thickness of a molecular layer may be, in principle, directly estimated from the ratio I/I_0. However, the thickness estimates may

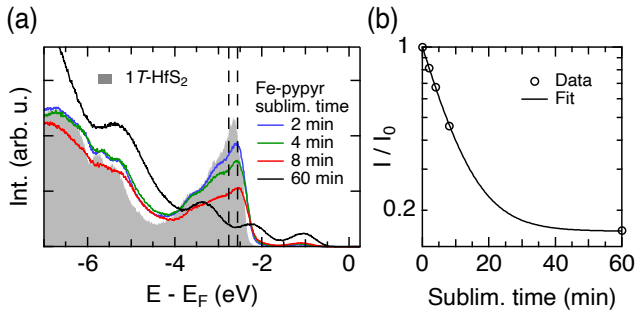

Figure 8: (a) VUV-ARPES spectra of Fe-pypyr on $1\,T$-HfS_2 for varying thicknesses (curves) along with a spectrum of the pristine substrate (gray area). The dashed lines delimit the energy range used for extracting the intensities I and I_0. (b) I/I_0 *versus* Fe-pypyr sublimation time (circles) along with a fit to Eq. 4 leading to $\lambda = 7.9 \pm 0.2$ min corresponding to 1.3 ± 0.1 ML. All data were acquired at room temperature.

be associated with significant errors. With increasing molecular-layer thicknesses, the photoemission signal on one hand decreases as the signal of the substrate is attenuated, and on the other hand increases due to photoemission from the molecular layer itself. The latter may become significant for binding energies exceeding 2 eV and is neglected in Eq. 3. We therefore developed an alternative method accounting for the signal originating from the molecular layer. The method is illustrated for Fe-pypyr on $1\,T$-HfS_2. The evaporation rate was ensured to remain constant over time using a quartz microbalance, such that the thickness of deposited molecules is proportional to time. VUV-ARPES spectra were acquired on the clean surface (gray area in Fig. 8a) and on the sample with increasing deposition time (lines in Fig. 8a). In contrast to the Au(111) substrate, there is no energy range where the substrate signal is large and the one from the molecular layer negligible. In analogy to the total electron yield of NEXAFS measurements,[37] the photoelectron intensity (at a given energy) reads:

$$I(d) = I_{\mathrm{ML}} \left[1 - \exp\left(-\frac{d}{\lambda}\right)\right] + I_0 \exp\left(-\frac{d}{\lambda}\right), \quad (4)$$

where I_0 and I_{ML} are respectively the intensities of a semi-infinite substrate and molecular layer. It should be noted that for $d \gg \lambda$, the layer may already be considered as semi infinite. We selected the integration range $[-2.76, -2.56]$ eV where the signal originating from the $1\,T$-HfS_2 substrate is large. In addition, I_{ML} and I_0 significantly differ in this energy range (compare intensity of the gray area and that of the black curve in Fig. 8a). Fig. 8b shows the evolution of the ratio I/I_0 as a function of the thickness of the molecular layer, expressed in sublimation time (at constant sublimation rate). A fit to the data using Eq. 4 results in a relative good agreement and $\lambda = 7.9 \pm 0.2$ min. Assuming that λ is the same on both samples, sublimation times can be converted to thicknesses. Furthermore, as the evaporation rate can be controlled by a quartz microbalance, molecular layers of desired thicknesses can be prepared. For example, with the experimental conditions of Fig. 8, growing a single monolayer takes $7.9/1.3 = 6.1$ min of deposition.

In the present study, we assumed that $\lambda = 1.3 \pm 0.1$ ML holds for all the investigated SCO complexes. We believe that this approximation is justified as long as the density of atoms with the layer are similar. Further detailed measurements of λ as shown in Fig. 7 on other molecular layers would be desirable in future work to verify this point. Accounting for uncertainties in the value of λ, we targeted $d \approx 0.5$ ML for the "sub-ML" samples to ensure that the complexes are in direct contact with the substrate.

Insights into the HS-to-LS relaxation dynamics

Besides providing static and stationary fractions of HS complexes, VUV-ARPES may also be employed to investigate switching and relaxation dynamics. Fig. 9a shows the temporal evolution of the HS fraction of 17 ML Fe-Bpzpypz on $1\,T$-HfS_2. The HS fraction is close to 100 % when the sample is illuminated with green light and exhibits an exponential decay upon turning off the green illumination. Interestingly, the time constant of the decays appears to increase as the VUV intensity is reduced (compare decays for VUV intensity of 100, 50 and 25 % in Fig. 9a). This suggests that the VUV light can induce HS-to-LS transitions, a process that we hereafter refer to as reverse-VUVIESST. A similar process, reverse-SOXIESST, has been reported for soft x-rays.[14]

Among the mechanisms involved in the HS-to-LS relaxation, we can identify: (i) the natural relaxation with a rate k^n_{HL} which solely depends on temperature, (ii) the VUVIESST effect with rate $k^{\mathrm{VUV}}_{\mathrm{LH}}$ leading to transitions from the LS to the HS state, and (iii) the reverse-VUVIESST effect with rate $k^{\mathrm{VUV}}_{\mathrm{HL}}$. Denoting γ_{HS} the HS fraction and neglecting cooperative effects, the rate equation reads:

$$\frac{d\gamma_{\mathrm{HS}}}{dt} = -\gamma_{\mathrm{HS}} \cdot k^n_{\mathrm{HL}} - \gamma_{\mathrm{HS}} \cdot k^{\mathrm{VUV}}_{\mathrm{HL}} + (1 - \gamma_{\mathrm{HS}}) \cdot k^{\mathrm{VUV}}_{\mathrm{LH}}. \quad (5)$$

Introducing $k^{\mathrm{eff}}_{\mathrm{HL}} = k^n_{\mathrm{HL}} + k^{\mathrm{VUV}}_{\mathrm{HL}} + k^{\mathrm{VUV}}_{\mathrm{LH}}$, the HS fraction has the evolution:

$$\gamma_{\mathrm{HS}}(t) = \frac{k^{\mathrm{VUV}}_{\mathrm{LH}}}{k^{\mathrm{eff}}_{\mathrm{HL}}} + \left(1 - \frac{k^{\mathrm{VUV}}_{\mathrm{LH}}}{k^{\mathrm{eff}}_{\mathrm{HL}}}\right) \cdot \exp\left(-k^{\mathrm{eff}}_{\mathrm{HL}} t\right), \quad (6)$$

where we assumed that $\gamma_{\mathrm{HS}} = 1$ at $t = 0$.

The HS fraction converges to $\approx$ 80, 70 and 65 % after relaxation under VUV illumination with 100, 50 and 25 % intensity, respectively. The stationary HS fraction in the absence of green light appears to depend on the VUV intensity. This can be rationalized from Eq. 6, which gives a HS fraction after relaxation ($t \to \infty$) of

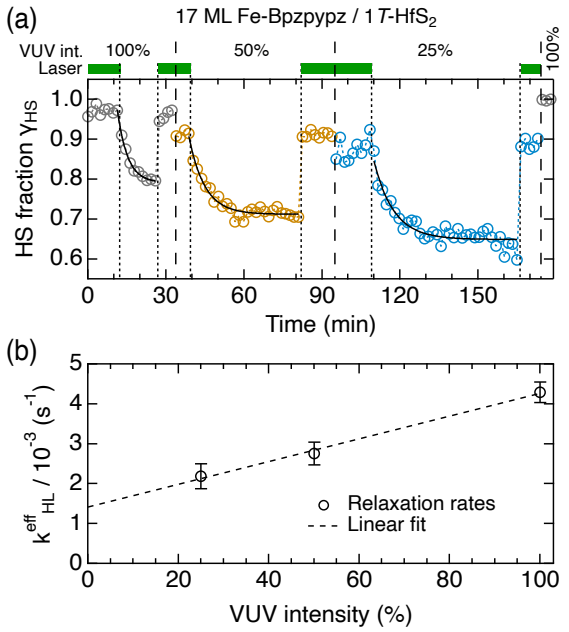

Figure 9: (a) Time evolution of the HS fraction of 17 ML Fe-Bpzpypz on 1 T-HfS_2 for different VUV-light intensities relative to the maximum intensity (25, 50 and 100 %) and with/without green laser light illumination (green rectangles represent the time during which illumination was on) along with fits to Eq. 6. (b) HS-to-LS relaxation rate k_{HL} as a function of the VUV intensity with corresponding linear fits (colored dashed lines). The sample temperature was about 20 K.

$k_{\mathrm{LH}}^{\mathrm{VUV}}/(k_{\mathrm{HL}}^{n} + k_{\mathrm{HL}}^{\mathrm{VUV}} + k_{\mathrm{LH}}^{\mathrm{VUV}})$. The rates $k_{\mathrm{LH/HL}}^{\mathrm{VUV}}$ most probably depend linearly on the VUV intensity in contrast to k_{HL}^{n}, which is expected to remain constant at a given temperature. As long as the natural relaxation rate is not negligible in comparison to the other involved rates, the HS fraction in the stationary regime is expected to depend on the VUV intensity. We note that the HS fraction upon relaxation with a VUV intensity of 100 % reaches ≈ 80 %, which is similar to saturation values found in SOXIESST experiments.[14,19,52]

Before further applying Eq. 6 to the data, we would like to point out that the relaxation did not systematically start with $\gamma_{\mathrm{HS}} = 1$ as we would expect when the sample is illuminated with green light. The initial HS fraction decreases as the VUV intensity is reduced (Fig. 9a). The decrease in VUV intensity was obtained by miss-aligning the monochromator whose purpose is to select a single spectral line of the He lamp. We believe that this action may have caused a small deviation of the VUV beam, thereby changing the spatial overlap with the green laser and effectively reducing the efficiency of the LIESST effect. We exclude beam-induced damage of the complexes as the HS-fraction evolution appears to be reproducible for a constant VUV intensity (see *e. g.*, gray circles in Fig. 9a). The HS fraction, however, abruptly drops when the VUV intensity is decreased (see *e. g.*, the drop at ≈35 min). This is consistent with a decrease of the overlap of the VUV and green-light beams on the sample surface. In the following, we therefore do not consider the absolute value of γ_{HS} but solely the time constants of the exponential decays.

The fit of the data shown in Fig. 9a using Eq. 6 gives effective relaxation rates $k_{\mathrm{HL}}^{\mathrm{eff}}$ of (4.3 ± 0.3), (2.8 ± 0.3) and $(2.2 \pm 0.4)\,10^{-3}\,\mathrm{s}^{-1}$ for VUV intensities of 100, 50 and 25 %, respectively (Fig. 9b). The evolution of $k_{\mathrm{HL}}^{\mathrm{eff}}$ is linear with the VUV intensity (see dashed line in Fig. 9), which suggests that $k_{\mathrm{HL}}^{\mathrm{VUV}} + k_{\mathrm{LH}}^{\mathrm{VUV}}$ is proportional to the VUV intensity. An estimate of the natural relaxation rate on the order of $10^{-3}\,\mathrm{s}^{-1}$ is obtained by extrapolating the data (dashed curve) to a VUV intensity of zero. We note that the value for the natural relaxation rate should be considered with caution because the linear fit is based on only three data points. Nonetheless, these series of experiments illustrate that VUV-ARPES is suited to retrieve dynamics of SCO systems, provided that the influence of the probe (here VUV light) on the investigated dynamics is characterized and accounted for.

A rough estimate of the VUVIESTT cross section is done as follows. The VUV flux at maximum intensity is on the order of $\Phi = 0.05\,\mathrm{s}^{-1}\,\mathrm{nm}^{-2}$. $k_{\mathrm{HL}}^{\mathrm{VUV}} + k_{\mathrm{LH}}^{\mathrm{VUV}} = k_{\mathrm{HL}}^{\mathrm{eff}} - k_{\mathrm{HL}}^{n} = 2.8 \times 10^{-3}\,\mathrm{s}^{-1}$ is inferred from the fit in Fig. 9b. Assuming $k_{\mathrm{HL}}^{\mathrm{VUV}}$ to be negligible in comparison to $k_{\mathrm{LH}}^{\mathrm{VUV}}$, we find a VUVIESST cross section $\sigma = k_{\mathrm{LH}}^{\mathrm{VUV}}/\Phi \approx 0.06\,\mathrm{nm}^2 = 6\,\mathrm{Å}^2$. Cross sections of $6\,\mathrm{Å}^2$ and $\approx 2\,\mathrm{Å}^2$ have been reported for the SOXIESST effect in Refs. 14 and 19, respectively. The similarity of the cross sections suggest that VUVIESST and SOXIESST share a common microscopic mechanism, and in particular that the photon energy is not crucial. A given molecule may be excited by absorption of an ultraviolet or a soft x-ray photon. The relaxation from the excited electronic state presumably leads to the emission of one or more energetic electrons, which in turn ionize neighboring molecules. Those ionized molecules may relax to the HS state. In addition, inelastic scattering of the secondary electrons with neutral molecules may also induce LS-to-HS transitions. The importance of secondary electrons for the SOXIESST effect has previously been evidenced in Refs. 14,19.

With the settings used for the present investigation, approximately 60–90 s of data acquisition was required to determine the HS fraction of the layer. However, much faster acquisition can be performed, in particular by reducing the energy range to the first two features used for the analysis and, due to the broad spectral features, worsening the energy resolution of the analyzer. Moreover, if the energy window of the analyzer is large enough, measurements can be performed with a fixed central kinetic energy to capture the spin state every few seconds.

Finally, ultrafast pump-probe measurements appear to be viable, as have been done for SCO complexes in the liquid,[76–80] and solid phase,[80–83] but not yet for SCO complexes on surfaces. At temperatures where the relaxation is sufficiently fast (microsecond timescale),

probing of the initial light-induced spin-state switching dynamics on sub-picosecond timescales may thus become possible.

Conclusions

We have evidenced that photoemission spectroscopy can be used to quantitatively determine the HS fraction of SCO layers. The technique is adapted to investigate sub-monolayers provided that adequate substrates are employed. In particular, we discuss in detail how the thickness of the layer can be reliably determined. Besides probing static and stationary states of the SCO films, we have shown that the method is also suitable for probing dynamics. While the HS-to-LS relaxation processes investigated here occur on the timescale of minutes, the technique has prospects to studying significantly faster dynamics.

Acknowledgements

We acknowledge funding from the German Research Foundation (DFG) via Sonderforschungsbereich 677 and project INST 257/442-1. The photoemission spectroscopy instrument ASPHERE III at beamline P04 of PETRA III (DESY) is funded by the Federal Ministry of Education and Research (BMBF) via contracts 05KS7FK2, 05K10FK1, 05K12FK1, and 05K13FK1 with Kiel University and contracts 05KS7WW1 and 05K10WW2 with the University of Würzburg.

References

1. Kahn, O.; Kröber, J.; Jay, C. Spin Transition Molecular Materials for displays and data recording. *Adv. Mater.* **1992**, *4*, 718–728.

2. Gütlich, P.; Garcia, Y.; Goodwin, H. A. Spin crossover phenomena in Fe (II) complexes. *Chem. Soc. Rev.* **2000**, *29*, 419–427.

3. Halcrow, M. A. *Spin-Crossover Materials: Properties and Applications*, 1st ed.; Wiley: Chichester, West Sussex, United Kingdom, 2013.

4. Molnár, G.; Salmon, L.; Nicolazzi, W.; Terki, F.; Bousseksou, A. Emerging properties and applications of spin crossover nanomaterials. *J. Mater. Chem. C* **2014**, *2*, 1360.

5. Kumar, K. S.; Ruben, M. Emerging trends in spin crossover (SCO) based functional materials and devices. *Coord. Chem. Rev.* **2017**, *346*, 176–205.

6. Molnár, G.; Rat, S.; Salmon, L.; Nicolazzi, W.; Bousseksou, A. Spin Crossover Nanomaterials: From Fundamental Concepts to Devices. *Adv. Mater.* **2017**, *2017*, 17003862.

7. Shi, S.; Schmerber, G.; Arabski, J.; Beaufrand, J.-B.; Kim, D. J.; Boukari, S.; Bowen, M.; Kemp, N. T.; Viart, N.; Rogez, G. *et al.* Study of molecular spin-crossover complex $Fe(phen)_2(NCS)_2$ thin films. *Appl. Phys. Lett.* **2009**, *95*, 043303.

8. Naggert, H.; Bannwarth, A.; Chemnitz, S.; von Hofe, T.; Quandt, E.; Tuczek, F. First observation of light-induced spin change in vacuum deposited thin films of iron spin crossover complexes. *Dalton Trans.* **2011**, *40*, 6364–6366.

9. Palamarciuc, T.; Oberg, J. C.; Hallak, F. E.; Hirjibehedin, C. F.; Serri, M.; Heutz, S.; Létard, J.-F.; Rosa, P. Spin crossover materials evaporated under clean high vacuum and ultra-high vacuum conditions: from thin films to single molecules. *J Mater Chem* **2012**, *22*, 9690–9695.

10. Ludwig, E.; Naggert, H.; Kalläne, M.; Rohlf, S.; Kröger, E.; Bannwarth, A.; Quer, A.; Rossnagel, K.; Kipp, L.; Tuczek, F. Iron(II) Spin-Crossover Complexes in Ultrathin Films: Electronic Structure and Spin-State Switching by Visible and Vacuum-UV Light. *Angew. Chem. - Int. Ed.* **2014**, *53*, 3019–3023.

11. Gruber, M.; Davesne, V.; Bowen, M.; Boukari, S.; Beaurepaire, E.; Wulfhekel, W.; Miyamachi, T. Spin state of spin-crossover complexes: From single molecules to ultrathin films. *Phys. Rev. B* **2014**, *89*, 195415.

12. Zhang, X.; Costa, P. S.; Hooper, J.; Miller, D. P.; N'Diaye, A. T.; Beniwal, S.; Jiang, X.; Yin, Y.; Rosa, P.; Routaboul, L. *et al.* Locking and Unlocking the Molecular Spin Crossover Transition. *Adv. Mater.* **2017**, *29*, 1702257.

13. Shalabaeva, V.; Rat, S.; Manrique-Juarez, M. D.; Bas, A.-C.; Vendier, L.; Salmon, L.; Molnár, G.; Bousseksou, A. Vacuum deposition of high-quality thin films displaying spin transition near room temperature. *J. Mater. Chem. C* **2017**, *5*, 4419–4425.

14. Kipgen, L.; Bernien, M.; Nickel, F.; Naggert, H.; Britton, A. J.; Arruda, L. M.; Schierle, E.; Weschke, E.; Tuczek, F.; Kuch, W. Soft-x-ray-induced spin-state switching of an adsorbed Fe(II) spin-crossover complex. *J. Phys.: Condens. Matter* **2017**, *29*, 394003.

15. Groizard, T.; Papior, N. R.; Le Guennic, B.; Robert, V.; Kepenekian, M. Enhanced Cooperativity in Supported Spin-Crossover Metal-Organic Frameworks. *J. Phys. Chem. Lett.* **2017**, *8*, 3415–3420.

16. Gruber, M.; Miyamachi, T.; Davesne, V.; Bowen, M.; Boukari, S.; Wulfhekel, W.; Alouani, M.; Beaurepaire, E. Spin crossover in $Fe(phen)_2(NCS)_2$ complexes on metallic surfaces. *J. Chem. Phys.* **2017**, *146*, 092312.

17. Rohlf, S.; Gruber, M.; Flöser, B. M.; Grunwald, J.; Jarausch, S.; Diekmann, F.; Kalläne, M.; Jasper-Toennies, T.; Buchholz, A.; Plass, W. *et al.* Light-Induced Spin Crossover in an Fe(II) Low-Spin Complex Enabled by Surface Adsorption. *J. Phys. Chem. Lett.* **2018**, *9*, 1491–1496.

18. Kumar, K. S.; Studniarek, M.; Heinrich, B.; Arabski, J.; Schmerber, G.; Bowen, M.; Boukari, S.; Beaurepaire, E.; Dreiser, J.; Ruben, M. Engineering On-Surface Spin Crossover: Spin-State Switching in a Self-Assembled Film of Vacuum-Sublimable Functional Molecule. *Adv. Mater.* **2018**, *30*, 1705416.

19. Wäckerlin, C.; Donati, F.; Singha, A.; Baltic, R.; Decurtins, S.; Liu, S.-X.; Rusponi, S.; Dreiser, J. Excited Spin-State Trapping in Spin Crossover Complexes on Ferroelectric Substrates. *J. Phys. Chem. C* **2018**, *122*, 8202–8208.

20. Atzori, M.; Poggini, L.; Squillantini, L.; Cortigiani, B.; Gonidec, M.; Bencok, P.; Sessoli, R.; Mannini, M. Thermal and light-induced spin transition in a nanometric film of a new high-vacuum processable spin crossover complex. *J. Mater. Chem. C* **2018**, *6*, 8885–8889.

21. Poggini, L.; Milek, M.; Londi, G.; Naim, A.; Poneti, G.; Squillantini, L.; Magnani, A.; Totti, F.; Rosa, P.; M. Khusniyarov, M. *et al.* Room temperature control of spin states in a thin film of a photochromic iron(ii) complex. *Mater. Horiz.* **2018**, *5*, 506–513.

22. Zhang, X.; N'Diaye, A. T.; Jiang, X.; Zhang, X.; Yin, Y.; Chen, X.; Hong, X.; Xu, X.; Dowben, P. A. Indications of magnetic coupling effects in spin cross-over molecular thin films. *Chem. Commun.* **2018**,

23. Rubio-Giménez, V.; Bartual-Murgui, C.; Galbiati, M.; Núñez-López, A.; Castells-Gil, J.; Quinard, B.; Seneor, P.; Otero, E.; Ohresser, P.; Cantarero, A. *et al.* Effect of nanostructuration on the spin crossover transition in crystalline ultrathin films. *Chem. Sci.* **2019**,

24. Ossinger, S.; Kipgen, L.; Naggert, H.; Bernien, M.; Britton, A. J.; Nickel, F.; Arruda, L. M.; Kumberg, I.; Engesser, T. A.; Golias, E. *et al.* Effect of ligand methylation on the spin-switching properties of surface-supported spin-crossover molecules. *J. Phys.: Condens. Matter* **2020**, *32*, 114003.

25. Ossinger, S.; Näther, C.; Buchholz, A.; Schmidtmann, M.; Mangelsen, S.; Beckhaus, R.; Plass, W.; Tuczek, F. Spin Transition of an Iron(II) Organoborate Complex in Different Polymorphs and in Vacuum-Deposited Thin Films: Influence of Cooperativity. *Inorg. Chem.* **2020**, *59*, 7966–7979.

26. Geest, E. P.; Shakouri, K.; Fu, W.; Robert, V.; Tudor, V.; Bonnet, S.; Schneider, G. F. Contactless Spin Switch Sensing by Chemo-Electric Gating of Graphene. *Adv. Mater.* **2020**, 1903575.

27. Lefter, C.; Rat, S.; Costa, J. S.; Manrique-Juárez, M. D.; Quintero, C. M.; Salmon, L.; Séguy, I.; Leichle, T.; Nicu, L.; Demont, P. *et al.* Current Switching Coupled to Molecular Spin-States in Large-Area Junctions. *Adv. Mater.* **2016**, *28*, 7508–7514.

28. Lefter, C.; Tan, R.; Dugay, J.; Tricard, S.; Molnár, G.; Salmon, L.; Carrey, J.; Nicolazzi, W.; Rotaru, A.; Bousseksou, A. Unidirectional Electric Field-Induced Spin-State Switching in Spin Crossover Based Microelectronic Devices. *Chem. Phys. Lett.* **2016**, *644*, 138–141.

29. Schleicher, F.; Studniarek, M.; Kumar, K. S.; Urbain, E.; Katcko, K.; Chen, J.; Frauhammer, T.; Hervé, M.; Halisdemir, U.; Kandpal, L. M. *et al.* Linking Electronic Transport through a Spin Crossover Thin Film to the Molecular Spin State Using X-ray Absorption Spectroscopy Operando Techniques. *ACS Appl. Mater. Interfaces* **2018**, *10*, 31580–31585.

30. Gee, A.; Jaafar, A. H.; Brachňaková, B.; Massey, J.; Marrows, C. H.; Šalitroš, I.; Kemp, N. T. Multilevel Resistance Switching and Enhanced Spin Transition Temperature in Single- and Double-Molecule Spin Crossover Nanogap Devices. *J. Phys. Chem. C* **2020**, *124*, 13393–13399.

31. Gopakumar, T. G.; Bernien, M.; Naggert, H.; Matino, F.; Hermanns, C. F.; Bannwarth, A.; Mühlenberend, S.; Krüger, A.; Krüger, D.; Nickel, F. *et al.* Spin-Crossover Complex on Au(111): Structural and Electronic Differences Between Mono- and Multilayers. *Chem. Eur. J.* **2013**, *19*, 15702–15709.

32. Gueddida, S.; Gruber, M.; Miyamachi, T.; Beaurepaire, E.; Wulfhekel, W.; Alouani, M. Exchange Coupling of Spin-Crossover Molecules to Ferromagnetic Co Islands. *J. Phys. Chem. Lett.* **2016**, *7*, 900–904.

33. Ossinger, S.; Naggert, H.; Kipgen, L.; Jasper-Toennies, T.; Rai, A.; Rudnik, J.; Nickel, F.; Arruda, L. M.; Bernien, M.; Kuch, W. *et al.* Vacuum-Evaporable Spin-Crossover Complexes in Direct

Contact with a Solid Surface: Bismuth versus Gold. *J. Phys. Chem. C* **2017**, *121*, 1210–1219.

34. Jasper-Tönnies, T.; Gruber, M.; Karan, S.; Jacob, H.; Tuczek, F.; Berndt, R. Deposition of a Cationic FeIII Spin-Crossover Complex on Au(111): Impact of the Counter Ion. *J. Phys. Chem. Lett.* **2017**, *8*, 1569–1573.

35. Knaak, T.; González, C.; Dappe, Y. J.; Harzmann, G. D.; Brandl, T.; Mayor, M.; Berndt, R.; Gruber, M. Fragmentation and Distortion of Terpyridine-Based Spin-Crossover Complexes on Au(111). *J. Phys. Chem. C* **2019**, *123*, 4178–4185.

36. Rohlf, S.; Grunwald, J.; Jasper-Toennies, T.; Johannsen, S.; Diekmann, F.; Studniarek, M.; Berndt, R.; Tuczek, F.; Rossnagel, K.; Gruber, M. Influence of Substrate Electronic Properties on the Integrity and Functionality of an Adsorbed Fe(II) Spin-Crossover Compound. *J. Phys. Chem. C* **2019**, *123*, 17774.

37. Gruber, M.; Berndt, R. Spin-Crossover Complexes in Direct Contact with Surfaces. *Magnetochemistry* **2020**, *6*, 35.

38. Gopakumar, T. G.; Matino, F.; Naggert, H.; Bannwarth, A.; Tuczek, F.; Berndt, R. Electron-Induced Spin Crossover of Single Molecules in a Bilayer on Gold. *Angew. Chem. - Int. Ed.* **2012**, *51*, 6262–6266.

39. Miyamachi, T.; Gruber, M.; Davesne, V.; Bowen, M.; Boukari, S.; Joly, L.; Scheurer, F.; Rogez, G.; Yamada, T. K.; Ohresser, P. *et al.* Robust spin crossover and memristance across a single molecule. *Nat. Commun.* **2012**, *3*, 938.

40. Bernien, M.; Wiedemann, D.; Hermanns, C. F.; Krüger, A.; Rolf, D.; Kroener, W.; Müller, P.; Grohmann, A.; Kuch, W. Spin Crossover in a Vacuum-Deposited Submonolayer of a Molecular Iron(II) Complex. *J. Phys. Chem. Lett.* **2012**, *3*, 3431–3434.

41. Bernien, M.; Naggert, H.; Arruda, L. M.; Kipgen, L.; Nickel, F.; Miguel, J.; Hermanns, C. F.; Krüger, A.; Krüger, D.; Schierle, E. *et al.* Highly Efficient Thermal and Light-Induced Spin-State Switching of an Fe(II) Complex in Direct Contact with a Solid Surface. *ACS Nano* **2015**, *9*, 8960–8966.

42. Bairagi, K.; Iasco, O.; Bellec, A.; Kartsev, A.; Li, D.; Lagoute, J.; Chacon, C.; Girard, Y.; Rousset, S.; Miserque, F. *et al.* Molecular-scale dynamics of light-induced spin cross-over in a two-dimensional layer. *Nat. Commun.* **2016**, *7*, 12212.

43. Bairagi, K.; Bellec, A.; Fourmental, C.; Iasco, O.; Lagoute, J.; Chacon, C.; Girard, Y.; Rousset, S.; Choueikani, F.; Otero, E. *et al.* Temperature-, Light-, and Soft X-ray-Induced Spin Crossover in a Single Layer of FeII-Pyrazolylborate Molecules in Direct Contact with Gold. *J. Phys. Chem. C* **2017**, *122*, 727.

44. Jasper-Toennies, T.; Gruber, M.; Karan, S.; Jacob, H.; Tuczek, F.; Berndt, R. Robust and Selective Switching of an FeIII Spin-Crossover Compound on Cu_2N/Cu(100) with Memristance Behavior. *Nano Lett.* **2017**, *17*, 6613.

45. Kipgen, L.; Bernien, M.; Ossinger, S.; Nickel, F.; Britton, A. J.; Arruda, L. M.; Naggert, H.; Luo, C.; Lotze, C.; Ryll, H. *et al.* Evolution of cooperativity in the spin transition of an iron(II) complex on a graphite surface. *Nat. Commun.* **2018**, *9*, 2984.

46. Fourmental, C.; Mondal, S.; Banerjee, R.; Bellec, A.; Garreau, Y.; Coati, A.; Chacon, C.; Girard, Y.; Lagoute, J.; Rousset, S. *et al.* Importance of Epitaxial Strain at a Spin-Crossover Molecule–Metal Interface. *J. Phys. Chem. Lett.* **2019**, *10*, 4103–4109.

47. Kumar, K. S.; Ruben, M. Sublimable Spin Crossover Complexes: From Spin-State Switching to Molecular Devices. *Angew. Chem. - Int. Ed.* **2021**, *60*, 7502–7521.

48. Köbke, A.; Gutzeit, F.; Röhricht, F.; Schlimm, A.; Grunwald, J.; Tuczek, F.; Studniarek, M.; Longo, D.; Choueikani, F.; Otero, E. *et al.* Reversible coordination-induced spin-state switching in complexes on metal surfaces. *Nat. Nanotechnol.* **2020**, *15*, 18–21.

49. Zhang, L.; Tong, Y.; Kelai, M.; Bellec, A.; Lagoute, J.; Chacon, C.; Girard, Y.; Rousset, S.; Boillot, M.; Rivière, E. *et al.* Anomalous Light-Induced Spin-State Switching for Iron(II) Spin-Crossover Molecules in Direct Contact with Metal Surfaces. *Angew. Chem. - Int. Ed.* **2020**, *59*, 13341–13346.

50. Maskowicz, D.; Sawczak, M.; Ghosh, A. C.; Grochowska, K.; Jendrzejewski, R.; Rotaru, A.; Garcia, Y.; Śliwiński, G. Spin Crossover and Cooperativity in Nanocrystalline [Fe(pyrazine)$Pt(CN)_4$] Thin Films Deposited by Matrix-Assisted Laser Evaporation. *Appl. Surf. Sci.* **2021**, *541*, 148419.

51. Sawczak, M.; Jendrzejewski, R.; Maskowicz, D.; Garcia, Y.; Dîrtu, M.; Kumar, V.; Śliwiński, G. Host–Guest Exchange Contribution to Transition Temperature Downshift in Nanocrystalline Fe(pyrazine)[$Pt(CN)_4$] Thin Films Prepared by Matrix-Assisted Pulsed Laser Evaporation. *J. Appl. Phys.* **2021**, *129*, 155308.

52. Davesne, V.; Gruber, M.; Miyamachi, T.; Da Costa, V.; Boukari, S.; Scheurer, F.; Joly, L.; Ohresser, P.; Otero, E.; Choueikani, F. *et al.* First glimpse of the soft x-ray induced excited spin-state trapping effect dynamics on spin cross-over molecules. *J. Chem. Phys.* **2013**, *139*, 074708–074708–6.

53. Davesne, V.; Gruber, M.; Studniarek, M.; Doh, W. H.; Zafeiratos, S.; Joly, L.; Sirotti, F.; Silly, M. G.; Gaspar, A. B.; Real, J. A. *et al.* Hysteresis and change of transition temperature in thin films of $Fe\{[Me_2Pyrz_3]BH\}_2$, a new sublimable spin-crossover molecule. *J. Chem. Phys.* **2015**, *142*, 194702.

54. Beniwal, S.; Sarkar, S.; Baier, F.; Weber, B.; Dowben, P. A.; Enders, A. Site selective adsorption of the spin crossover complex $Fe(phen)_2(NCS)$ on Au(111). *J. Phys.: Condens. Matter* **2020**, *32*, 324003.

55. Brandl, T.; Johannsen, S.; Häussinger, D.; Suryadevara, N.; Prescimone, A.; Bernhard, S.; Gruber, M.; Ruben, M.; Berndt, R.; Mayor, M. Iron in a cage: fixation of a Fe(II)tpy2 complex by fourfold interlinking. *Angew. Chem. - Int. Ed.* **2020**, *59*, 15947–15952.

56. Collison, D.; Garner, C. D.; McGrath, C. M.; Mosselmans, J. F. W.; Roper, M. D.; Seddon, J. M. W.; Sinn, E.; Young, N. A. Soft X-ray induced excited spin state trapping and soft X-ray photochemistry at the iron $L_{2,3}$ edge in $[Fe(phen)_2(NCS)_2]$ and $[Fe(phen)_2(NCSe)_2]$ (phen = 1,10-phenanthroline). *J. Chem. Soc., Dalton Trans.* **1997**, 4371–4376.

57. Real, J. A.; Muñoz, M. C.; Faus, J.; Solans, X. Spin Crossover in Novel Dihydrobis(1-pyrazolyl)borate $[H_2B(pz)_2]$-Containing Iron(II) Complexes. Synthesis, X-ray Structure, and Magnetic Properties of $[FeL\{H_2B(pz)_2\}_2]$ (L = 1,10-Phenanthroline and 2,2‘-Bipyridine). *Inorg. Chem.* **1997**, *36*, 3008–3013.

58. Neese, F. The ORCA Program System. *Wiley Interdiscip. Rev. Comput. Mol. Sci.* **2012**, *2*, 73–78.

59. Neese, F. Software Update: the ORCA Program System, Version 4.0. *Wiley Interdiscip. Rev. Comput. Mol. Sci.* **2018**, *8*, e1327.

60. Rappe, A. K.; Casewit, C. J.; Colwell, K. S.; Goddard, W. A.; Skiff, W. M. UFF, a Full Periodic Table Force Field for Molecular Mechanics and Molecular Dynamics Simulations. *J. Am. Chem. Soc.* **1992**, *114*, 10024–10035.

61. Hanwell, M. D.; Curtis, D. E.; Lonie, D. C.; Vandermeersch, T.; Zurek, E.; Hutchison, G. R. Avogadro: an Advanced Semantic Chemical Editor, Visualization, and Analysis Platform. *J. Cheminformatics* **2012**, *4*, 17.

62. Stewart, J. J. P. Optimization of Parameters for Semiempirical Methods VI: More Modifications to the NDDO Approximations and Re-Optimization of Parameters. *J. Mol. Model.* **2012**, *19*, 1–32.

63. Stewart, J. J. P. MOPAC2016. 2016; `http://openmopac.net`.

64. Becke, A. D. Density-Functional Thermochemistry. III. The Role of Exact Exchange. *J. Chem. Phys.* **1993**, *98*, 5648–5652.

65. Lee, C.; Yang, W.; Parr, R. G. Development of the Colle-Salvetti Correlation-Energy Formula into a Functional of the Electron Density. *Phys. Rev. B* **1988**, *37*, 785–789.

66. Stephens, P. J.; Devlin, F. J.; Chabalowski, C. F.; Frisch, M. J. Ab Initio Calculation of Vibrational Absorption and Circular Dichroism Spectra Using Density Functional Force Fields. *J. Phys. Chem.* **1994**, *98*, 11623–11627.

67. Weigend, F.; Ahlrichs, R. Balanced Basis Sets of Split Valence, Triple Zeta Valence and Quadruple Zeta Valence Quality for H to Rn: Design and Assessment of Accuracy. *Phys. Chem. Chem. Phys.* **2005**, *7*, 3297–3305.

68. Weigend, F. Accurate Coulomb-Fitting Basis Sets for H to Rn. *Phys. Chem. Chem. Phys.* **2006**, *8*, 1057–1065.

69. Grimme, S.; Antony, J.; Ehrlich, S.; Krieg, H. A Consistent and Accurate Ab Initio Parametrization of Density Functional Dispersion Correction (DFT-D) for the 94 Elements H-Pu. *J. Chem. Phys.* **2010**, *132*, 154104.

70. Grimme, S.; Ehrlich, S.; Goerigk, L. Effect of the Damping Function in Dispersion Corrected Density Functional Theory. *J. Comput. Chem.* **2011**, *32*, 1456–1465.

71. Reiher, M.; Salomon, O.; Artur Hess, B. Reparameterization of Hybrid Functionals Based on Energy Differences of States of Different Multiplicity. *Theor. Chem. Acc.* **2001**, *107*, 48–55.

72. Cartier dit Moulin, C.; Rudolf, P.; Flank, A. M.; Chen, C. T. Spin Transition Evidenced by Soft X-ray Absorption Spectroscopy. *J. Phys. Chem.* **1992**, *96*, 6196–6198.

73. Seah, M. P.; Dench, W. A. Quantitative electron spectroscopy of surfaces: A standard data base for electron inelastic mean free paths in solids. *Surf. Interface Anal.* **1979**, *1*, 2–11.

74. Hauser, A. *Spin Crossover in Transition Metal Compounds II*; Topics in Current Chemistry 234; Springer Berlin Heidelberg, 2004; pp 155–198.

75. Traving, M.; Seydel, T.; Kipp, L.; Skibowski, M.; Starrost, F.; Krasovskii, E. E.; Perlov, A.; Schattke, W. Combined photoemission and inverse photoemission study of HfS_2. *Phys. Rev. B* **2001**, *63*, 035107.

76. Bressler, C.; Milne, C.; Pham, V.-T.; ElNahhas, A.; Veen, R. M. v. d.; Gawelda, W.; Johnson, S.; Beaud, P.; Grolimund, D.; Kaiser, M. *et al.* Femtosecond XANES Study of the Light-Induced Spin Crossover Dynamics in an Iron(II) Complex. *Science* **2009**, *323*, 489–492.

77. Huse, N.; Kim, T. K.; Jamula, L.; McCusker, J. K.; de Groot, F. M. F.; Schoenlein, R. W. Photo-Induced Spin-State Conversion in Solvated Transition Metal Complexes Probed via Time-Resolved Soft X-ray Spectroscopy. *J. Am. Chem. Soc.* **2010**, *132*, 6809–6816.

78. Cannizzo, A.; Milne, C.; Consani, C.; Gawelda, W.; Bressler, C.; van Mourik, F.; Chergui, M. Light-Induced Spin Crossover in Fe(II)-Based Complexes: The Full Photocycle Unraveled by Ultrafast Optical and X-ray Spectroscopies. *Coord. Chem. Rev.* **2010**, *254*, 2677–2686.

79. Auböck, G.; Chergui, M. Sub-50-fs Photoinduced Spin Crossover in $[Fe(bpy)_3]^{2+}$. *Nat. Chem.* **2015**, *7*, 629–633.

80. Chergui, M.; Collet, E. Photoinduced Structural Dynamics of Molecular Systems Mapped by Time-Resolved X-ray Methods. *Chem.l Rev.* **2017**, *117*, 11025–11065.

81. Collet, E.; Moisan, N.; Baldé, C.; Bertoni, R.; Trzop, E.; Laulhé, C.; Lorenc, M.; Servol, M.; Cailleau, H.; Tissot, A. *et al.* Ultrafast Spin-State Photoswitching in a Crystal and Slower Consecutive Processes Investigated by Femtosecond Optical Spectroscopy and Picosecond X-ray Diffraction. *Phys. Chem. Chem. Phys.* **2012**, *14*, 6192–6199.

82. Lorenc, M.; Balde, C.; Kaszub, W.; Tissot, A.; Moisan, N.; Servol, M.; Buron-Le Cointe, M.; Cailleau, H.; Chasle, P.; Czarnecki, P. *et al.* Cascading Photoinduced, Elastic, and Thermal Switching of Spin States Triggered by a Femtosecond Laser Pulse in an Fe(III) Molecular Crystal. *Phys. Rev. B* **2012**, *85*, 054302.

83. Ridier, K.; Bas, A.; Shalabaeva, V.; Nicolazzi, W.; Salmon, L.; Molnár, G.; Bousseksou, A.; Lorenc, M.; Bertoni, R.; Collet, E. *et al.* Finite Size Effects on the Switching Dynamics of Spin-Crossover Thin Films Photoexcited by a Femtosecond Laser Pulse. *Adv. Mater.* **2019**, *31*, 1901361.

TOC Graphic

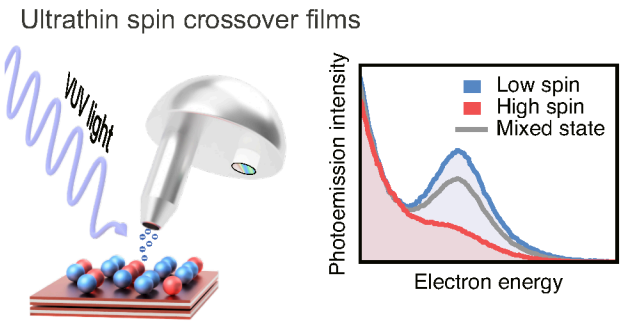
Ultrathin spin crossover films
hν light
Photoemission intensity
Low spin
High spin
Mixed state
Electron energy